IJNRD.ORG **ISSN : 2456-4184**

INTERNATIONAL JOURNAL OF NOVEL RESEARCH AND DEVELOPMENT (IJNRD) | IJNRD.ORG

An International Open Access, Peer-reviewed, Refereed Journal

Synthesis of Composite photocatalyst containing carbon nitride and metal phthalocyanine using mechanochemical methods

1.Adeniji R.A   2.Olaseinde K.F

1. School of Chemistry
University of Lincoln

2. Department of Physics
Federal University of Technology Akure, Nigeria

ABSTRACT

Two potential photocatalytic material were synthesized and characterized using mechanochemical method. We describe two molecular metal phthalocyanine with a carboxylic acid group attachment (MPcCOOH; M = Cu, Co) that is ball-milled with a Sulphur-doped carbon nitride (SCN_x). Two different pathways were taken to synthesized the Sulphur-doped carbon nitride and were named SCN_{x-1} and SCN_{x-2} respectively. The resulting four composites (SCN_x|MPcCOOH) were characterized using the Spectrum 100 spectrometer made by PERKINS which scanned the FT-IR in the ATR-IR mode. The presence of a carboxylic acid is acknowledged by the spectra and it conforms with results presented in the literature. There a band stretching at around 600-700 cm^{-1} in all the composite material indicating a functionalization of the Sulphur addition. Surface reorganization of the O-H functional group is noticeable at around 3500 cm^{-1} and also amide stretching indication the presence of carbonyl group in both materials understudy. This work ultimately portrays the huge potential of these materials; however, Cu-derivatives show a distinctive characteristic after it is ball-milled.

Key words: Photocatalytic, mechanochemical, Perkins, phthalocyanine, Sulphur

INTRODUCTION

Change in the average weather condition of the world has been the prominent bone of contention for humanity in the last few decades. The average temperature is rising alarmingly, with around 1.08°C higher than the last decade's average (Menne *et al.,* 2018). The primary cause of this erratic increment in the global temperature is the surge in the earthly energy demand, which is achieved through the burning of fossils. The combustion process of burning fossil fuels emits CO2, which is not fully reduced by the natural process of the carbon circle. Other anthropogenic greenhouse gasses are also the cause of a warmer earth. According to Eurostat, fossil fuels (such as coal, natural gas, and oil) made up 72.3% of the EU's total inland energy consumption in 2020. Without an understanding of the chemistry of the atmosphere, the effect of these greenhouse gases on the rise in the average global cannot be properly appreciated.

The atmosphere is composed of many gases, but nitrogen (N_2) and oxygen (O_2) are the two most prevalent ones. Almost 78% of the atmosphere is made up of nitrogen, while only 21% of oxygen. Other gases like argon, carbon dioxide, neon, helium, and methane (CH_4) make up the final 1% of the atmosphere. Water vapor (H_2O), which is crucial for the water cycle and weather patterns, and ozone (O_3), which shields life on Earth from the damaging ultraviolet (UV) radiation, are the other trace gases found in the atmosphere. The approximate value of the amount of solar energy reaching the Earth from a mean distance of the sun is 1366 Wm^{-2} (Gueymard, 2004). However, only two-thirds of this energy reaches the Earth, while the rest is reflected back into space.

The remaining high-energy UV radiation that reaches the Earth is absorbed by the ozone layer, which forms a protective barrier that serves as a natural shield and transforms it into heat. Particularly, UV-C and most UV-B rays with wavelengths of less than 120 – 290 nm are the most dangerous types of UV radiation, and they are absorbed by ozone (O_3) molecules in the stratosphere. UV radiation causes the splitting of ozone molecules, resulting in the formation of an oxygen molecule (O_2) and an oxygen atom (O). This reaction absorbs the energy of the UV radiation, preventing it from reaching the Earth's surface. The ozone-oxygen cycle is then finished when the oxygen atom (O) reacts with another ozone molecule (O_3) to produce two oxygen molecules (O_2). As shown in the following equations (Portmann *et al.,* 2012):

$$O_3 + UV\ radiation \rightarrow O_2 + O \qquad\qquad (1.1)$$

$$O + O_3 \rightarrow 2O_2 \qquad\qquad (1.2)$$

$$3O_2 + UV\ radiation \rightarrow 2O_3 \qquad\qquad (1.3)$$

Equation 1 represents the absorption, equation 2 represents the formation of the new oxygen, and the last equation represents the formation of the new ozone. However, it has been discovered that a number of man-made substances, including sulfur dioxide (SO_2), nitrogen oxides (NOx), and chlorofluorocarbons (CFCs), can damage ozone molecules and contribute to the thinning of the ozone layer. The ozone layer is essential for shielding life on Earth from UV radiation, which can destroy organisms and cause skin cancer, cataracts, and other illnesses in people and other animals. As a result, international accords like the Montreal Protocol were developed with the intention of gradually ending the manufacturing and use of ozone-depleting compounds. Also, the scientific community is geared to provide alternative means of producing energy, such as developing renewable energies.

1. LITERATURE REVIEW– CO_2 REDUCTION FOR SUSTAINABLE FUEL PRODUCTION WITH MODIFIED CARBON NITRIDE & COBALT PHTHALOCYANINE

An appealing way through photocatalytic reduction of CO_2 to produce storable fuels is to capture it and eventually use it to implement a carbon-neutral energy cycle. The development of efficient, long-lasting, and financially viable catalysts and light absorbers is at the core of research on solar fuels' use of CO_2. Recently, it has become clear that hybrid photosynthetic systems with molecular catalysts immobilized on solid supports (light-absorbing semiconductors or dye-sensitized semiconductors) are a promising approach for suspension-based photoreactor applications because they combine the selectivity of molecules with the durability of heterogeneous materials (Dalle et al., 2019). Graphitic carbon nitride (g-CNx), which can absorb both UV and visible light and is resilient to photochemical conditions, has recently gained attention as a promising semiconductor for photocatalytic processes like water splitting and CO2 reduction. With a suitably low conduction band energy minimum (@1.10 V vs. NHE at pH 6.6) and a moderately small band gap, g-CNx can absorb UV/Vis light and then reduce a surface tension (Liu *et al.,* 2015).

In CNx-based photocatalytic systems for CO2 reduction, a variety of co-catalysts have been used, such as weakly anchoring Ruthenium (Ru) complexes or (Ruthenium Rhenium) Ru-Re dyads functionalized with phosphonic acid (Maeda et al., 2013), Nanowires made of sodium niobite, molecular cobalt and iron complexes in solution, metalloporphyrins covalently grafted on CNx, single-atom cobalt sites built into the compound, single-atom cobalt sites (Shi et al., 2014). Here, the photocatalytic conversion of it stated how to convert CO_2 to CO using a robust organic-inorganic hybrid material. The polymeric cobalt phthalocyanine (CoPPc; PPc stands for polymeric phthalocyanine) is activated by solar radiation being absorbed by mesoporous carbon nitride (mpg-CNx) catalyst that has been deposited on the surface as show in Fig. 1.6 In situ polymerization causes CoPPc to be deposited on mpg-CNx and is a successful method for immobilization of a catalyst. VB and CB stand for the valence and conduction bands, respectively, in Figure 1.7 below, which shows a schematic representation of the light-driven CO2 reduction catalysed by the mpg-CNx CoPPc hybrid
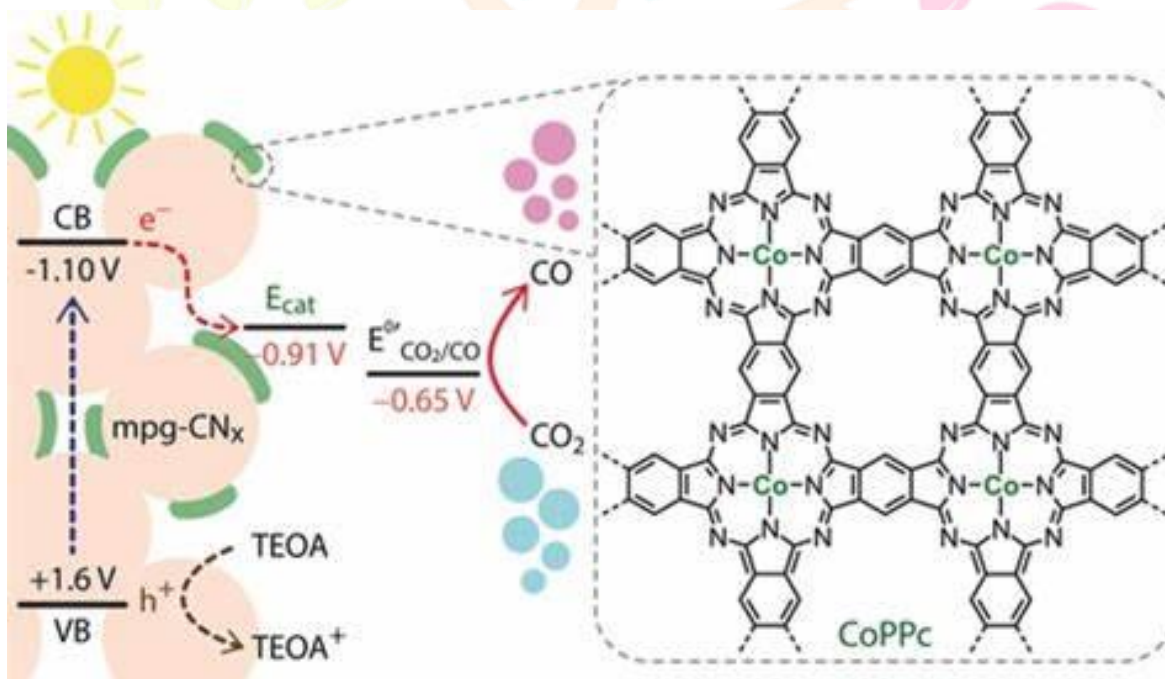
Fig. 1. A pictorial representation of the light-driven CO2 reduction catalysed by the mpg-CNx CoPPc hybrid (Wiley, 2019).

Copper also exhibits distinctive characteristics in its ability to catalyse electrochemical reactions conversion of CO_2 into alcohols, hydrocarbons, and other compounds with a maximum of three carbon atoms (Kuh et al., 2012). The primary outcomes of the copper-mediated CO_2 reduction reaction (CO2RR) consist of C_2 products. Both ethylene and

ethanol possess a substantial worth for the chemical and fuel sectors. Ethylene possesses potential as a viable means of producing various chemical intermediates, utilizing ethylene oligomerization, such as polyethylene, ethylene oxide, and diesel.

Additionally, ethanol may be utilized as a chemical feedstock with similar applications. Ethene, glycol ethers, amines, and esters have found utility as solvents and fuels within the contexts of various scientific and industrial fields. The utilization of copper for product selectivity presents a persistent challenge.

The carbon dioxide reduction reaction (CO2RR) on copper produces a variety of C_1, C_2, and C_3 compounds in addition to hydrogen, ethylene, and ethanol, according to empirical studies (Kuh et al., 2012). The link between C_1 and C_2/C_3 production is greatly influenced by copper's surface shape, according to Hori et al. (2003). Compared to the tightly packed Cu (111) facet, the Cu (100) surface with more openness exhibits increased selectivity towards products containing C-C bonds. An important finding about Cu-based catalysts is that in order to produce ethylene and ethanol with a considerable degree of selectivity, strong overpotentials must be applied, which prevents the development of by-products (Figueiredo et al., 2016).

The study conducted by Kortlever et al. (2015) examined the capability of the material in exhibiting selectivity towards H_2, $HCOO-$, and CH_4. The elements have piqued academic interest in the investigation of potential mechanisms that aid the CO_2 reduction response (CO2RR) and the fundamental processes that control it. Significant challenges have been faced in experimental research into the underlying processes driving CO_2 reduction reactions (CO2RR). Variable numbers of electrons and protons must participate in the CO_2 electroreduction process in order to generate the desired products. Based on the main products they produce; Three groups can be made up of elemental metallic catalysts. These include the creation of cobalt (Co), lead (Pb), bismuth (Bi), tin (Sn), indium (In), and zinc (Zn) using gold (Au), silver (Ag), palladium (Pd), and zinc (Zn). Mercury (Hg) for the synthesis of formic acid/formate, and copper (Cu) to produce a variety of hydrocarbons. Despite showing notable selectivity for a variety of compounds, the catalysts are still insufficient for practical deployment as posited by Bridja (2020).

The process of Carbon dioxide (CO_2) reduction electrochemically can progress through multiple pathways of reduction, involving a range of two (2) to eighteen (18) electrons, leading to the formation of diverse end products

such as methanol (CH_3OH), carbon monoxide (CO), methane (CH_4), and formic acid (HCOOH)/formate (HCOO),

and acetic acid. Chemical compounds such as acetic acid (CH_3COOH), ethanal (CH_3CHO), ethanol (CH_3CH_2OH),

ethylene (CH_2CH_2), and various other substances belong to the category of organic compounds. Table 1 presents a

compilation of the reactions that have been reported with the highest frequency.

REACTIONS	(V vs. RHE) = E^0
$2H^+ + 2e^- \rightarrow H_2$	0.00
$CO_2 + 2H^+ + 2e^- \rightarrow CO + H_2O$	−0.10
$CO_2 + 2H^+ + 2e^- \rightarrow HCOOH$	−0.12
$CO_2 + 6H^+ + 6e^- \rightarrow CH_3OH + H_2O$	+0.03
$CO_2 + 8H^+ + 8e^- \rightarrow CH_4 + 2H_2O$	+0.17
$2CO_2 + 8H^+ + 8e^- \rightarrow CH_3COOH + 2H_2O$	+0.11
$2CO_2 + 10H^+ + 10e^- \rightarrow CH_3CHO + 3H_2O$	+0.06
$2CO_2 + 12H^+ + 12e^- \rightarrow CH_3CH_2OH + 3H_2O$	+0.09
$2CO_2 + 12H^+ + 12e^- \rightarrow C_2H_4 + 4H_2O$	+0.08
$3CO_2 + 18H^+ + 18e^- \rightarrow CH_3CH_2CH_2OH + 5H_2O$	+0.10

Table 1. Equilibrium potentials for electrochemical processes.

2. METHODS AND MATERIALS

This section presents the synthesis methods for producing a composited photocatalyst using Sulphur-doped carbon nitride and carboxylic acid functionalized metal phthalocyanine. An explanation of its physicochemical characteristics and photocatalytic potentials, precisely carbon dioxide (CO_2) reduction. It also contains an overview of some characterization techniques that are adopted in the study of materials' microstructure, morphology and optical properties.

a) Chemical Used : The reagents used in this study and their respective suppliers are listed in the Table 2. below

REAGENTS	SUPPLIER
1. N, N-dimethyl formamide [68-12-2]	Sigma - Aldrich corporation
2. Melamine [108-78-1]	
3. tri-thiocyanuric acid [638-16-4]	
4. Thiourea [62-56-6]	
5. Trimellitic acid anhydride (2.6 mmol, 0.5 g)	
6. Cobalt(ii) acetate tetrahydrate (1.28 mmol, 0.32 g)	
7. Ammonium chloride (1.9 mmol, 102 mg)	
8. Urea (16.6 mmol, 1 g)	
9. Ammonium heptamolybdate (0.042 mmol, 0.050 g)	
10. Nitrobenzene	
11. Diethylether	
12. Copper (II) acetate tetrahydrate (1.28 mmol, 0.32 g)	

Table. 2. Table of Reagent

b) synthesis of Sulphur Doped Carbon Nitride

To create homogeneous solutions, melamine (1.000 g, 8 mmol) and tri-thiocyanuric acid (1.410 g, 8 mmol) were mixed into 50.0 mL of distilled water (DI water) and 25.0 mL of N, N-dimethyl formamide, respectively. The resulting aqueous melamine solution was added dropwise to the tri-thiocyanuric acid solution and agitated for 0.5 hours at 200 rpm to produce a light-yellow mixture. This combination was then swirled for another 6 hours at 80 °C to produce supramolecular aggregate. 250 mL DI water was added to the mixed solution after it had cooled to room temperature (20 °C), and it was then agitated for another 12 hours in an ambient environment. Vacuum filtration was used to collect the light-yellow product, which was then baked at 60 °C for 12 hours to dry it (Wang et al., 2018). The solid underwent annealing annealed under aerobic condition in a furnace at 550 °C for 4 h (heating rate of 5 °C min^{-1}) to yield a yellow product named as SCN_{x-1} as depicted in Fig 2.1.
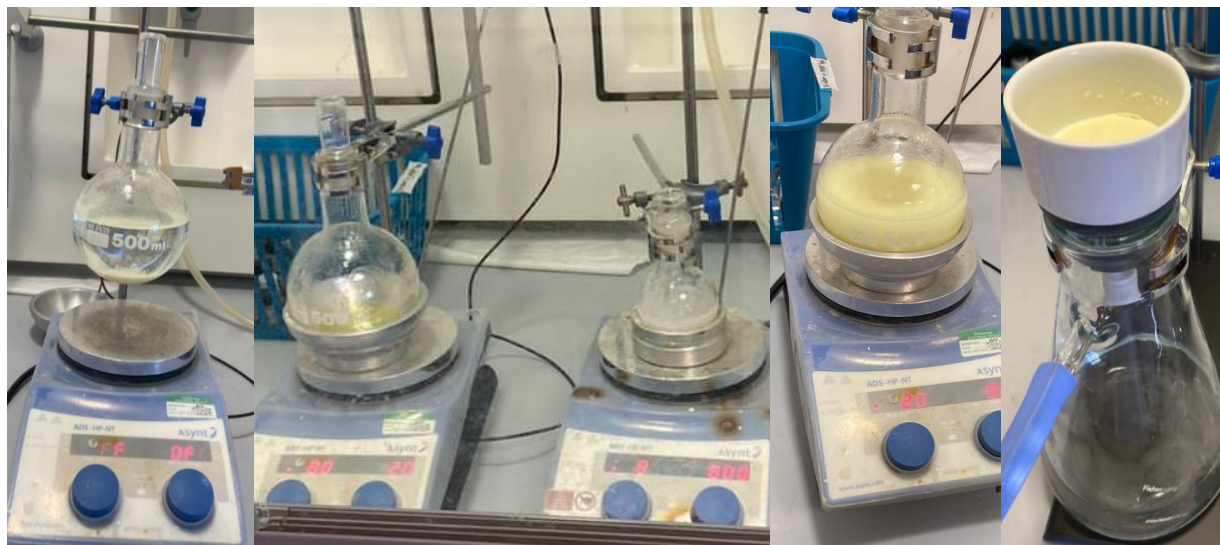
Plate 1. Pictures of the steps taken in the synthesisation of SCN$_{x-1}$

c. Method 2 (Thiourea precursor)

Thiourea (10g) was heated at 550 °C for 4 h in air at a heating rate of 5 °C/min (Lv et al., 2020). The resulting yellow powder was ground using an agate mortar and pestle. Material named as SCN$_{x-2}$ which is shown in Fig 2.2

Plate 2. Picture of SCNx-2 after it was heated.

d. Synthesis of Cobalt Phthalocyanine(CoPc-COOH)

Trimellitic acid anhydride (2.6 mmol, 0.5 g), cobalt (II) acetate tetrahydrate (1.28 mmol, 0.32 g), ammonium chloride (1.9 mmol, 102 mg), urea (16.6 mmol, 1 g), and ammonium heptamolybdate (0.042 mmol, 0.050 g) were first ground into a solid mixture in an agate mortar. Then, the mixture was transferred to a Schlenk flask, 5 ml nitrobenzene was added, and the mixture was purged with N$_2$. The mixture was refluxed overnight. After cooling, the mixture was then

diluted with diethylether and filtered. The precipitate was then suspended in aqueous KOH solution (80 mL, 1 M) and heated for 12 h at 80 °C under stirring. The hydrolysed product was precipitated by adding concentrated hydrochloric acid (10 mL) and then filtered. The supernatant was discarded, and the solid residue was washed with H2O for five times to reach neutral pH. The resulting sample was dried under vacuum to afford the title compound as a blue-green solid (Shang et al., 2022).

e. Sythensis of copper Phthaylocyanine(CuPc-CooH)

Trimellitic acid anhydride (2.6 mmol, 0.5 g), copper (II) acetate tetrahydrate (1.28 mmol, 0.32 g), ammonium chloride (1.9 mmol, 102 mg), urea (16.6 mmol, 1 g), and ammonium heptamolybdate (0.042 mmol, 0.050 g) were first ground into a solid mixture in an agate mortar. Then, the mixture was transferred into a 20 mL glass vial and heated at 180 °C for 2 h in a muffle furnace. Next, the dark solid was dispersed in water with sonication and centrifuged (7155 g, 10 min). The supernatant was discarded. The precipitate was dissolved in 40 mL of aqueous KOH (1 M) and heated for 12 h at 80 °C with stirring. The hydrolysed product was then precipitated by adding 10 mL of concentrated hydrochloric acid and centrifuged (7155 g, 10 min). The precipitate was washed with water five times to reach a neutral pH and dried in air.

e. Balling Methods

Ball milling is the process of grinding flakes to the desired powder size. Fig. 2.3 shows where the raw material would be fed into a big spinning cylinder loaded with steel balls. The rods stand inside the framework while the cylinder spins, creating a cascading impression of steel balls. The varying impact of the balls produces a crushing action, reducing the amount of coarse powder. Once the particles have been reduced to the correct size, they are propelled by the downstream blower's airflow. Many final product qualities (density, dimensional variation, strength, compressibility, and so on) are determined by the ball mill process.

The operator modifies the following ball mill settings based on the particle size and density distribution results: intake speed, air flow, and ball level. Fig. 2.3 is an image of a ball milling machine.
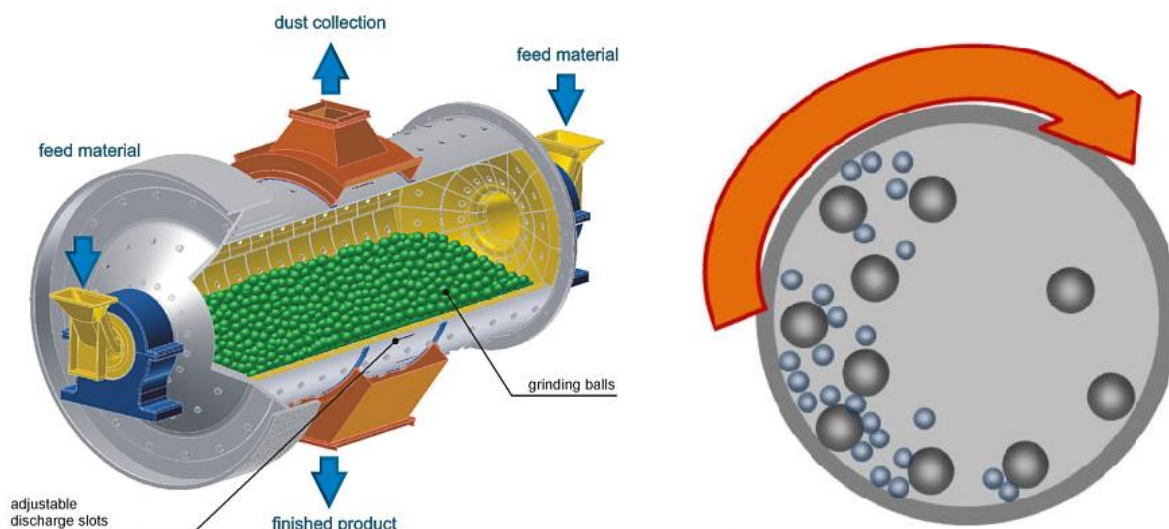
Fig. 2. Schematic illustration of a ball milling machine and the ball-milling process showing its impact on the ductility of the spherical particles (Jung et al., 2013)

The ball milling operation is critical since it determines many characteristics of the final products (density, dimensional change, green strength, compressibility, etc.). Based on the size distribution and density results, the operator adjusts the following ball mill parameters: feed rate, air flow rate and level of balls.

After the sulphur doped carbon nitride and the metal-catalyst has been synthesised. 100 mg of bulk carbon nitride, 5 mg CoPcCOOH/CuPcCOOH, and 0.1 mL DMF were ball milled with stainless steel balls (3 balls in each container) for 30min at 25 Hz. The resultant powder was collected using ethanol, filtered using a membrane filter, and washed thoroughly with DMF (3x5 ml) and ethanol (5x5 ml).

The mechanochemically generated materials using ball milling method are given in Table 2.1 below:

S/N	Material abbreviation	Carbon nitride	Catalyst
1	$SCN_{x-1}|CoPcCOOH$	SCN_{x-1}	CoPcCOOH
2	$SCN_{x-2}|CoPcCOOH$	SCN_{x-2}	CoPcCOOH
3	$SCN_{x-1}|CuPcCOOH$	SCN_{x-1}	CuPcCOOH
4	$SCN_{x-2}|CuPcCOOH$	SCN_{x-2}	CuPcCOOH

Table 3: List of the materials understudy.

3.   RESULTS AND DISCUSSIONS

The main result obtained is to describe the physical, morphological characteristics and the reaction mechanism of these heterogeneous catalysts, hence, the primary characterization techniques employed is the Attenuated total reflectance infrared (ATR-IR) whose analyses are given below. The analyses are solemnly based on the description of the functional group(s) present in the materials understudy, to describe the overall spectra peaks, to describe the observable changes in the spectra peaks, the intensity and adsorption characteristics, the surface reaction observed and the photocatalytic pathways in corelation with the photocatalytic performance of the materials.

A.   FT-IR   SPECTRA   OF   SULPHUR-DOPED   CARBON   NITRIDE   AND   COBALT PHTHALOCYANINE PHOTOCATALYST

The experimental ATR-IR spectra of CoPcCOOH was consistent with the one reported in literature (Roy & Reisner, 2019; Xiao et al., 2018). The noticeable difference is due to the ethanol that was used in the collection of the catalyst after ball milling, hence the presence of O-H stretching vibration as shown in Fig 3. We observed small differences in the ATR spectra between the SCN_{x-1} and $SCN_{x-1}|CoPcCOOH$ nanocomposites. These differences are related to the presence of CoPc molecules attached to the SCN_{x-1} surface. The O–H stretching vibrations were detected at 3200 to 3350 cm^{-1}. A peak around 1350-1400 cm^{-1} is found which corresponds to C-N stretching vibrations in the cobalt phthalocyanine core (Shang et al., 2022).

The principal bands (absorption bands) observed in the $SCN_{x-1}|CoPcCOOH$ spectra at around 600-700 cm^{-1} corresponding to C-S stretching vibrations of the Sulphur-containing functional groups adsorption.
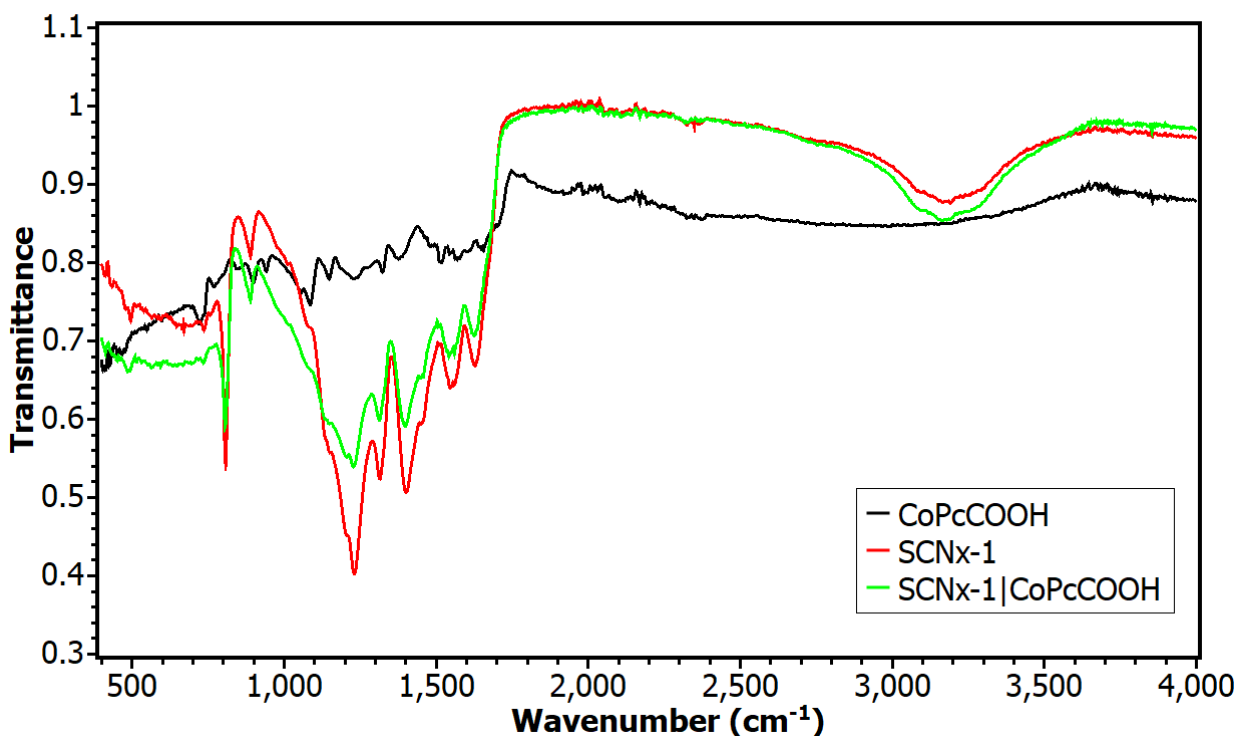
Fig 3 FT-IR spectra of melamine precursor sulphur-doped carbon nitride, CoPcCOOH and SCNx-1|CoPcCOOH

As seen in Fig 3, a prominent peak at 1600 cm^{-1} indicates the existence of aromatic C=C bonds. Aromatic C-H stretching vibrations, on the other hand, are not shown. Knowing how the modifier is deposited on the catalytically active metal surface is critical for understanding asymmetric catalysis on modified metals phthalocyanine (Manbeck & Fujita, 2015).

The spectra in Fig. 3 and 4 are identical, however, the proportion of IR transmitted is higher in the thiourea precursor (SCN$_{x-2}$). A surface reorganisation of the O-H groups explained the signals of the positive signal at 3200 cm^{-1} being coupled with a negative signal at 3500 cm^{-1}. In Fig. 4, an amide stretching is detected about 1660-1690 cm^{-1}, confirming the presence of a carbonyl group.

The -C=O bands in Fig.4 are crisp and strong, at roughly 1646 and 1688 cm^{-1}, indicating overlap of the -C=O of amide and -C=O of -COOH for both the CoPcCOOH and SCN$_{x-2}$|CoPcCOOH before functionalization.
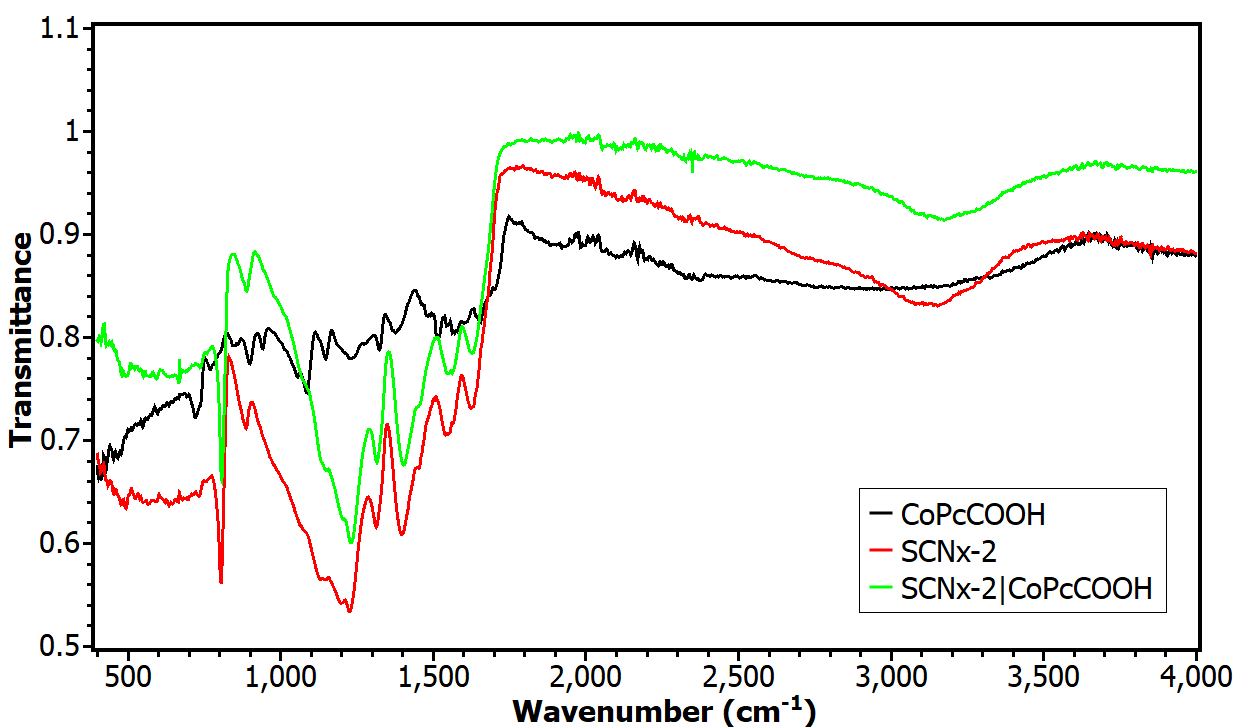
Fig 4. FT-IR spectra of Sulphur-doped carbon nitride, CoPcCOOH and SCNx-2|CoPcCOOH

After it has been functionalized, the creation of another C=O of an amide group may be responsible for the small shift. The amide N-H stretch in the SCN$_{x-2}$|CoPcCOOH is represented by the band at 1556 cm^{-1}. Similarly, for SCN$_{x-1}$|CoPcCOOH and SCN$_{x-2}$|CoPcCOOH, a shift from 1688 cm^{-1} to 1660 cm^{-1} was observed, resulting from the

transformation of the -C=O of -COOH to the -C=O of amide, Fig. 4, while the band at 1250 cm^{-1} (Fig. 3) was observed at 1200 cm^{-1} (Fig. 4), due to the amide N-H stretch.

B. FT-IR SPECTRA OF SULPHUR-DOPED CARBON NITRIDE AND COPPER PHTHALOCYANINE PHOTOCATALYST

When the catalyst was exposed to the ethanol feed, changes in the relative intensities of the bands were detected when compared with the pure liquid phase spectra (Figueiredo et al., 2016). A comparison of spectra following the ball-milling of SCN$_{x-1}$ and CuPcCOOH is shown in Fig 5. Bands at 1650, 1900 and an intensely broad spectra at 3450 cm^{-1} were observed not to be in the fingerprint region in the CuPcCOOH spectra, whereas in the fingerprint region spectra, bands at 750, 1200, 1350, and 1400 cm^{-1} were also observed.
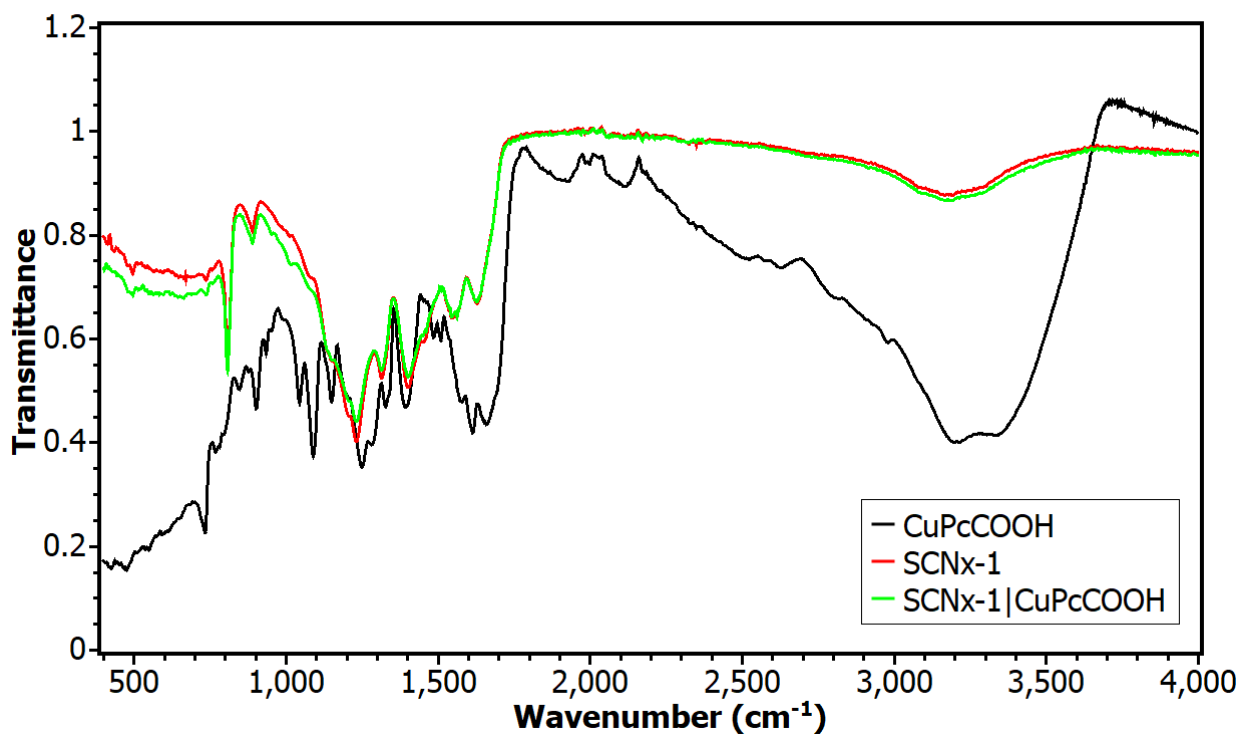
Fig 5. FT-IR spectra of Sulphur-doped carbon nitride, CuPcCOOH and SCN$_{x-1}$|CuPcCOOH

The stretching bands observed in the CuPcCOOH had disappeared in the SCN$_{x-1}$|CuPcCOOH spectra. It is evident that bands that are present on CuPcCOOH are lost when CN is pre-adsorbed on the catalyst. The increase in the intensity in the fingerprint region in the SCN$_{x-1}$|CuPcCOOH can be further attributed to this adsorption, as observed Fig 5.

The FT-IR spectra of SCN$_{x-2}$, the carboxylic acid-functionalized nanoparticles and their respective phthalocyanine nanocomposites are presented, Fig.6. Most of the vibrational bands of interest could not be undisputedly assigned due to the absorption of N–H and O–H bands which are around the same region. For instance, the SCN$_{x-1}$|CuPcCOOH in Fig.4, possess both N–H and O–H functional groups in SCN$_{x-2}$|CuPcCOOH Fig 5, suggesting that the bands at above 3200 cm^{-1} may be due to the overlap absorption of N–H and O–H stretching modes. Also, in the SCN$_{x-}$

$_2$|CuPcCOOH nanocomposites (Fig. 5), because not all of the carboxylic acid sites on each nanoparticle are anticipated to be involved in the amide bond formation, some O-H groups on the surface of the nanoparticles are likely to remain unbound. As a result, the bands above 3200 cm^{-1} in the nanohybrids might be attributed to the overlap absorption of the free NH ends of the SCN$_{x-1}$|CuPcCOOH, as well as the nanoparticles' free O-H and N-H. The proposed numerous absorptions might therefore explain the observed band broadness at > 3200 cm^{-1}.
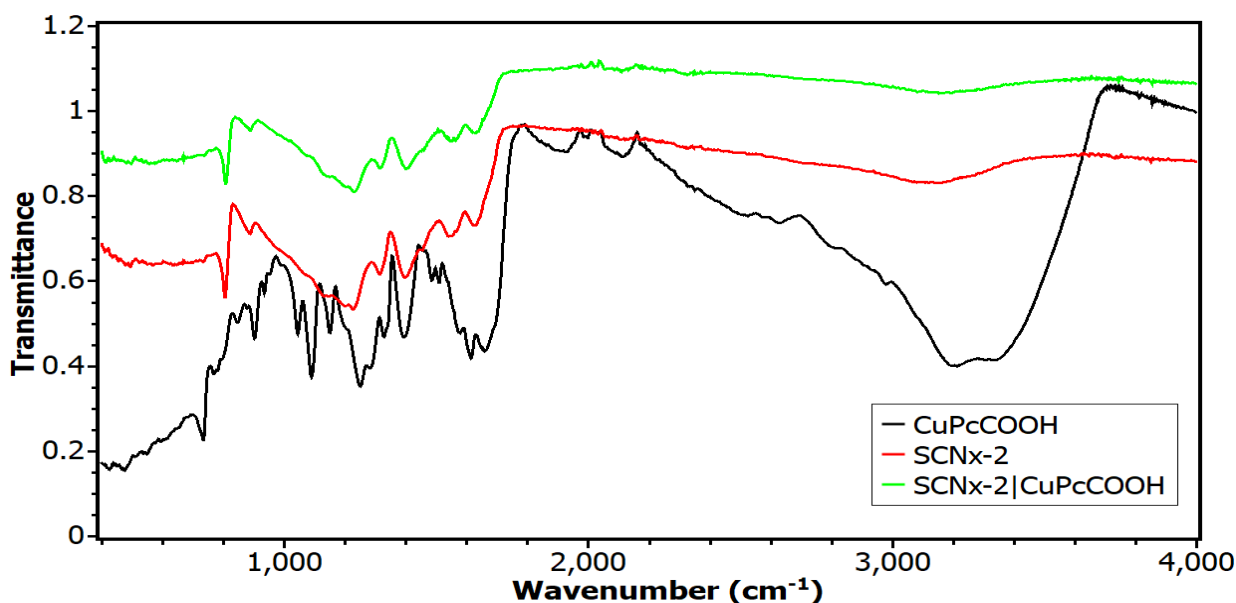
Fig.6 FT-IR spectra of Sulphur-doped carbon nitride, CuPcCOOH and SCN$_{x-2}$|CuPcCOOH composite.

The FT-IR spectrum of the SCN$_{x-1}$|CuPcCOOH and SCN$_{x-2}$|CuPcCOOH nanocomposite showed generally similar vibrational modes, therefore, making it difficult to identify the vibrational bands responsible for the amide linkages, Fig.5. The FT-IR spectra (Fig.5) showed the expected vibrational bands in all the CuPcCOOH (Chen et al., 1993; Liu et al., 2023). The ─C=O stretching bands due to the amide linkage were not so distinct, because of the overlap absorption of the N─H stretching and bending modes which are present in both the SCN$_{x-1}$|CuPcCOOH and the SCN$_{x-2}$|CuPcCOOH.

The other characteristic carboxylic group vibrations such as C─O stretching, (C─O) and in-plane ─C─O─H bending, (C─O─H) modes are expected between 1150 and 1450 cm^{-1} region. The bands at 200 and 400 cm^{-1} in the SCN$_{x-2}$|CuPcCOOH nano-catalyst may be attributed to Cu-C stretching vibrations, while 300 and 500 cm^{-1} are caused by Cu-N bending (Z. Liu et al., 2023). However, these bands interact with various bands that are aromatic, making their clear assignment problematic. Furthermore, because these bands are lacking in the core SCN$_{x-2}$, they might be

attributed to C-N absorption. Because these bands are strikingly lacking in the spectra of CuPcCOOH, the extra bands at 2563, 2750, and 2875 cm^{-1} may account for the structural variations produced by the existence of the SCN$_{x-2}$ monolayer. This shows that the bands at 2563, 2750, and 2875 cm^{-1} were caused by the S-S interaction of the thiol group SCN$_{x-2}$ (Abu-Sari et al., 2023).

C. COMPARATIVE DIFFERENCE OF THE EFFECTS OF SULPHUR DOPED CARBON NITRIDE ON TWO METAL PHTHALOCYANINES CATALYST

Figure 4 below shows the comparison of the results of all the studied compound, it is observed that each if the compound has its uniqueness in the fingerprint region that is the region less than 1500 cm^{-1} which contains a lot of bands, it would be daunting to interpret these observed spectra in this region however they show similar spectra due to the similarity in the constituent materials.
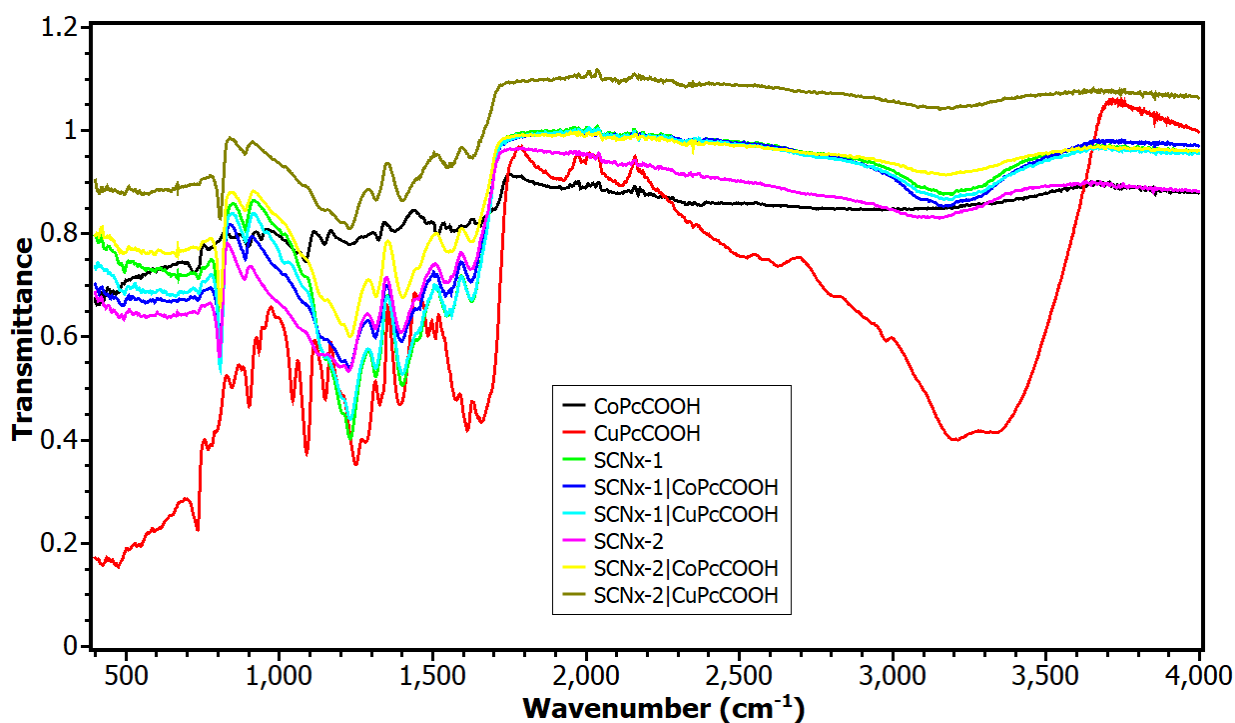
Fig. 7: FT-IR spectra of Sulphur-doped carbon nitride, MPcCOOH and MPcCOOH composite photocatalyst.

The major differences are depicted in the 100 - 500 cm^{-1} region, the strong bands in the region 125–550 cm^{-1} and 3000–3500 cm^{-1} for MPcCOOH(s) may be attributed to the carboxylic group. Bands associated with copper-ligand vibrations, such as Cu-N and Cu-C bonds are present in 250 cm-1 and 400 cm^{-1} respectively, this is due to copper-carbon stretching vibrations. there is a shift in nitrogen-based vibrations due to the influence of copper, around 1050 cm^{-1}. The changes in C-H stretching vibrations around 3250 cm^{-1} due to distortion in the copper coordination (Z. Liu et al., 2023). This is also evident in the result of the CoPcCOOH, however it is not as glaring as it is in the CuPcCOOH.

Similar bands in CuPcCOOH core–shell are noticeable on comparing the relative intensities with that of CoPcCOOH., but have been greatly attenuated by the more intense bands attributed to the SCN_{x-1} substrate. A series of peaks ranging between 1200 and 1700 cm−1 are typical stretching vibration modes of the dramatic C-N and C-N heterocycles. The broad absorption peak around 3200 cm^{-1} originates from the N H and O H bond stretching vibrations (Yan et al., 2009). All the characteristic vibration peaks of Co CN are the same as the pure CN except a slightly lower intensity at around 3200 cm^{-1}, suggested that the addition of CoPcCOOH even facilitated the deamination process during the self-polymerization of melamine at high temperatures. It is also notable that the spectra of SCN_{x-1}|CuPcCOOH and SCN_{x-2}|CuPcCOOH are similar, suggesting that phthalocyanine CuPcCOOH as the additive in the precursor had no obvious influence on the typical structure of the SCN_{x-1} and SCN_{x-2}. The results also show that the addition of CoPc speeds up the deamination process during melamine self-polymerization at high temperatures (Liu et al., 2019).

The key similarities between the two potential photocatalysts are the amine functional group properties. Amine N-H stretches are significantly narrower and less severe than -OH stretches, often appearing in the 3300-3500 cm^{-1} range. Primary amines have two amine hydrogens and two N-H stretches. Secondary amines have a single amine hydrogen and one N-H stretch. Tertiary amines have no absorption in this area because the amine nitrogen contains no hydrogen atoms. The NH stretches in an amide occur in the same 3300-3500 cm^{-1} range.

4. CONCLUSION

The Research focuses on the synthesis and analysis of photocatalysts composed of a combination of sulphur-doped carbon nitride (SCN_x) and carboxylic acid functionalized metal phthalocyanine (MPcCOOH). The main aim of this study was to investigate the influence of sulphur incorporation into carbon nitride on the photocatalytic CO_2 reduction process, specifically in the presence of two different metal phthalocyanines: cobalt phthalocyanine (CoPcCOOH) and copper phthalocyanine (CuPcCOOH). The examination and comprehension of these mixed photocatalysts yielded valuable details about their structure and functional features. The principal characterisation approach was Attenuated Total Reflectance Infrared (ATR-IR) spectroscopy, which allowed the identification of different functional groups contained in the materials, the detection of molecular vibrations, and the assessment of surface contacts between the composite materials. The ATR-IR spectra of pure metal phthalocyanines and their composite photocatalysts exhibited considerable changes and shifts in characteristic bands, suggesting good functionalization and interaction between the components. The ATR-IR spectroscopy results have provided valuable insights into the structural changes and interactions within the composites. Due to residual ethanol from the ball-milling process, the presence of O-H stretching vibrations in the CoPcCOOH photocatalysts was detected. Shifts in C-N stretching vibrations and the appearance of discrete bands associated with the amide group were signs of good functionalization. Similarly, the ATR-IR spectra of CuPcCOOH catalyst indicated alterations in vibrational bands associated with the carboxylic group and copper-ligand interactions, demonstrating the excellent integration of SCN_x with phthalocyanine.

5. RECOMMENDATION

To analyse materials more thoroughly, it is imperative to use additional characterization methods in addition to FT-IR spectroscopy. Techniques such as XRD, SEM, TEM, and XPS can reveal materials' structure, shape, and elemental content. Investigate how functional groups, metal centres, and surface contacts affect catalysis. However, this may require advanced spectroscopic methods like in-situ FT-IR or X-ray absorption.

Nanocomposite materials' surface area and porosity affect photocatalytic activity, examining it using technique such as Brunauer-Emmett-Teller (BET) analysis would give more insightful results about the photocatalytic performance of Sulphur-doped carbon nitride with carboxylic functionalized metal phthalocyanine (SCNx|MPcCOOH). Assess photocatalyst stability and recyclability over time.

Lastly, it is necessary to examine the materials' ability to degrade organic contaminants, produce hydrogen, and other processes. By conducting in-depth kinetic research to understand reaction rates and mechanisms. To further explore if these metal phthalocyanines and carbon nitride-based compounds could be used in water purification, air pollution control, and carbon capture and conversion.

REFERENCES

Adhigan Murali, M. A. K., Nitride, N. G. C., Akyüz, D., Keleş, T., Biyiklioglu, Z., & Koca, A. (2022). Metallophthalocyanines bearing polymerizable [5-((1E)-[4-(diethylamino) phenyl] methylene amino)-1-naphthy1] oxy groups as electrochemical pesticide sensor. *Electroanalysis*, *29*, 2913–2924.

Aresta, M., Dibenedetto, A., & Angelini, A. (2014). Catalysis for the Valorization of Exhaust Carbon: From CO2 to Chemicals, Materials, and Fuels. Technological Use of CO2. *Chemical Reviews*, *114*(3), 1709–1742. https://doi.org/10.1021/cr4002758

Barber, J., & Tran, P. D. (2013). From natural to artificial photosynthesis. *Journal of the Royal Society, Interface*, *10*(81), 20120984. https://doi.org/10.1098/rsif.2012.0984

Belver, C., Bedia, J., Gómez-Avilés, A., Peñas-Garzón, M., & Rodriguez, J. J. (2019). Chapter 22—Semiconductor Photocatalysis for Water Purification. In S. Thomas, D. Pasquini, S.-Y. Leu, & D. A. Gopakumar (Eds.), *Nanoscale Materials in Water Purification* (pp. 581–651). Elsevier. https://doi.org/10.1016/B978-0-12-813926-4.00028-8

Bonegardt, D., Klyamer, D., Köksoy, B., Durmuş, M., & Basova, T. (2020). Hybrid materials of carbon nanotubes with fluoroalkyl- and alkyl-substituted zinc phthalocyanines. *Journal of Materials Science: Materials in Electronics*, *31*(14), 11021–11028. https://doi.org/10.1007/s10854-020-03650-x

Chen, H., Wang, M., Feng, L., & Yang, S. (1993). Synthesis and photoconductivity study of phthalocyanine polymers. II. PVK-co-CuPc (COOH)3. *Journal of Polymer Science Part A: Polymer Chemistry*, *31*(5), 1165–1170. https://doi.org/10.1002/pola.1993.080310511

Chen, P.-W., Li, K., Yu, Y.-X., & Zhang, W.-D. (2017). Cobalt-doped graphitic carbon nitride photocatalysts with high activity for hydrogen evolution. *Applied Surface Science*, *392*, 608–615. https://doi.org/10.1016/j.apsusc.2016.09.086

Comeau, Z. J., Facey, G. A., Harris, C. S., Shuhendler, A. J., & Lessard, B. H. (2020). Engineering Cannabinoid Sensors through Solution-Based Screening of Phthalocyanines. *ACS Applied Materials & Interfaces*, *12*(45), 50692–50702. https://doi.org/10.1021/acsami.0c17146

Dalle, K. E., Warnan, J., Leung, J. J., Reuillard, B., Karmel, I. S., & Reisner, E. (2019). Electro- and Solar-Driven Fuel Synthesis with First Row Transition Metal Complexes. *Chemical Reviews*, *119*(4), 2752–2875. https://doi.org/10.1021/acs.chemrev.8b00392

Del Caño, T., Parra, V., Rodríguez-Méndez, M. L., Aroca, R. F., & De Saja, J. A. (2005). Characterization of evaporated trivalent and tetravalent phthalocyanines thin films: Different degree of organization. *Applied Surface Science*, *246*(4), 327–333. https://doi.org/10.1016/j.apsusc.2004.11.036

El-Nahass, M. M., El-Gohary, Z., & Soliman, H. S. (2003). Structural and optical studies of thermally evaporated CoPc thin films. *Optics & Laser Technology*, *35*(7), 523–531. https://doi.org/10.1016/S0030-3992(03)00068-9

Farag, A. A. M. (2007). Optical absorption studies of copper phthalocyanine thin films. *Optics & Laser Technology*, *39*(4), 728–732. https://doi.org/10.1016/j.optlastec.2006.03.011

Figueiredo, M. C., Ledezma-Yanez, I., & Koper, M. T. M. (2016). In Situ Spectroscopic Study of CO2 Electroreduction at Copper Electrodes in Acetonitrile. *ACS Catalysis*, *6*(4), 2382–2392. https://doi.org/10.1021/acscatal.5b02543

Garba, M. D., Usman, M., Khan, S., Shehzad, F., Galadima, A., Ehsan, M. F., Ghanem, A. S., & Humayun, M. (2021). CO2 towards fuels: A review of catalytic conversion of carbon dioxide to hydrocarbons. *Journal of Environmental Chemical Engineering*, *9*(2), 104756. https://doi.org/10.1016/j.jece.2020.104756

Ghani, F., Kristen, J., & Riegler, H. (2012). Solubility Properties of Unsubstituted Metal Phthalocyanines in Different Types of Solvents. *Journal of Chemical & Engineering Data*, *57*(2), 439–449. https://doi.org/10.1021/je2010215

Gonçalves, J. M., Martins, P. R., Rocha, D. P., Matias, T. A., Julião, M. S. S., Munoz, R. A. A., & Angnes, L. (2021). Recent trends and perspectives in electrochemical sensors based on MOF-derived materials. *Journal of Materials Chemistry C*, *9*(28), 8718–8745. https://doi.org/10.1039/D1TC02025K

Grant, T. M., McIntyre, V., Vestfrid, J., Raboui, H., White, R. T., Lu, Z.-H., Lessard, B. H., & Bender, T. P. (2019). Straightforward and Relatively Safe Process for the Fluoride Exchange of Trivalent and Tetravalent Group 13 and 14 Phthalocyanines. *ACS Omega*, *4*(3), 5317–5326. https://doi.org/10.1021/acsomega.8b03202

Gueymard, C. A. (2004). The sun's total and spectral irradiance for solar energy applications and solar radiation models. *Solar Energy*, *76*(4), 423–453. https://doi.org/10.1016/j.solener.2003.08.039

Guo, S., Zhu, Y., Yan, Y., Min, Y., Fan, J., & Xu, Q. (2016). Holey structured graphitic carbon nitride thin sheets with edge oxygen doping via photo-Fenton reaction with enhanced photocatalytic activity. *Applied Catalysis B: Environmental*, *185*, 315–321. https://doi.org/10.1016/j.apcatb.2015.11.030

Hori, Y., Takahashi, I., Koga, O., & Hoshi, N. (2003). Electrochemical reduction of carbon dioxide at various series of copper single crystal electrodes. *Journal of Molecular Catalysis A: Chemical*, *199*(1), 39–47. https://doi.org/10.1016/S1381-1169(03)00016-5

Jhong, H.-R. "Molly," Ma, S., & Kenis, P. J. (2013). Electrochemical conversion of CO2 to useful chemicals: Current status, remaining challenges, and future opportunities. *Current Opinion in Chemical Engineering*, *2*(2), 191–199. https://doi.org/10.1016/j.coche.2013.03.005

Jin, W. X., Ma, S. Y., Tie, Z. Z., Li, W. Q., Luo, J., Cheng, L., Xu, X. L., Wang, T. T., Jiang, X. H., & Mao, Y. Z. (2015). Synthesis of hierarchical SnO2 nanoflowers with enhanced acetic acid gas sensing properties. *Applied Surface Science*, *353*, 71–78. https://doi.org/10.1016/j.apsusc.2015.06.089

Jung, Y., Erickson, E., Ding, B., Kim, S., Woo, S.-K., & Lee, J.-K. (2013). Microstructure and electrical conductivity in shape and size controlled molybdenum particle thick film. *Journal of Materials Science*, *48*, 3760–3768. https://doi.org/10.1007/s10853-013-7175-2

Khan, M. M. (2021). Chapter 1—Principles and mechanisms of photocatalysis. In M. Sakar, R. G. Balakrishna, & T.-O. Do (Eds.), *Photocatalytic Systems by Design* (pp. 1–22). Elsevier. https://doi.org/10.1016/B978-0-12-820532-7.00008-4

Kortlever, R., Shen, J., Schouten, K. J. P., Calle-Vallejo, F., & Koper, M. T. M. (2015). Catalysts and Reaction Pathways for the Electrochemical Reduction of Carbon Dioxide. *The Journal of Physical Chemistry Letters*, *6*(20), 4073–4082. https://doi.org/10.1021/acs.jpclett.5b01559

Kruchinin, V. N., Klyamer, D. D., Spesivtsev, E. V., Rykhlitskii, S. V., & Basova, T. V. (2018). Optical Properties of Thin Films of Zinc Phthalocyanines Determined by Spectroscopic Ellipsometry. *Optics and Spectroscopy*, *125*(6), 1019–1024. https://doi.org/10.1134/S0030400X18120093

Kumar, C. V., Sfyri, G., Raptis, D., Stathatos, E., & Lianos, P. (2014). Perovskite solar cell with low cost Cu-phthalocyanine as hole transporting material. *RSC Advances*, *5*(5), 3786–3791. https://doi.org/10.1039/C4RA14321C

Kuprikova, N. M., Klyamer, D. D., Sukhikh, A. S., Krasnov, P. O., Mrsic, I., & Basova, T. V. (2020). Fluorosubstituted lead phthalocyanines: Crystal structure, spectral and sensing properties. *Dyes and Pigments*, *173*, 107939. https://doi.org/10.1016/j.dyepig.2019.107939

Lin, B., Xue, C., Yan, X., Yang, G., Yang, G., & Yang, B. (2015). Facile fabrication of novel SiO2/g-C3N4 core–shell nanosphere photocatalysts with enhanced visible light activity. *Applied Surface Science*, *357*, 346–355. https://doi.org/10.1016/j.apsusc.2015.09.041

Liu, Q., Gao, L., Su, X., Zhou, F., & Duan, G. (2019). Interfacial self-assembly of CoPc thin films with their high sensing use as NO2 sensors. *Materials Chemistry and Physics*, *234*, 94–101. https://doi.org/10.1016/j.matchemphys.2019.05.029

Liu, Z., Wu, M., & Ma, J. (2023). Cu–N4 in copper phthalocyanine@CFC catalyst for ammonia oxidation reaction catalysis. *Physical Chemistry Chemical Physics*, *25*(11), 7859–7868. https://doi.org/10.1039/D2CP05589A

Löbbert, G. (2000). Phthalocyanines. In *Ullmann's Encyclopedia of Industrial Chemistry*. John Wiley & Sons, Ltd. https://doi.org/10.1002/14356007.a20_213

Lokesh, K. S., Shivaraj, Y., Dayananda, B. P., & Chandra, S. (2009). Synthesis of phthalocyanine stabilized rhodium nanoparticles and their application in biosensing of cytochrome c. *Bioelectrochemistry*, *75*(2), 104–109. https://doi.org/10.1016/j.bioelechem.2009.02.005

Lougdali, M., Zazoui, M., Abboud, Y., Bouari, A. E., Zawadzka, A., Płóciennik, P., Strzelecki, J., Strzałkowski, K., Migalska-Zalas, A., Waszkowska, K., Sahraoui, B., & El kouari, Y. (2022). Linear and nonlinear optical properties of Manganese bis-(8- hydroxyquinoline) thin films for optoelectronic devices: Experimental and computational studies. *Journal of Molecular Structure*, *1249*, 131558. https://doi.org/10.1016/j.molstruc.2021.131558

Lv, H., Huang, Y., Koodali, R. T., Liu, G., Zeng, Y., Meng, Q., & Yuan, M. (2020). Synthesis of Sulfur-Doped 2D Graphitic Carbon Nitride Nanosheets for Efficient Photocatalytic Degradation of Phenol and Hydrogen Evolution. *ACS Applied Materials & Interfaces*, *12*(11), 12656–12667. https://doi.org/10.1021/acsami.9b19057

Maeda, K., Sekizawa, K., & Ishitani, O. (2013). A polymeric-semiconductor–metal-complex hybrid photocatalyst for visible-light CO2 reduction. *Chemical Communications*, *49*(86), 10127–10129. https://doi.org/10.1039/C3CC45532G

Maitra, U., Lingampalli, S. R., & Rao, C. N. R. (2014). Artificial photosynthesis and the splitting of water to generate hydrogen. *Current Science*, *106*(4), 518–527.

Manbeck, G. F., & Fujita, E. (2015). A review of iron and cobalt porphyrins, phthalocyanines and related complexes for electrochemical and photochemical reduction of carbon dioxide. *Journal of Porphyrins and Phthalocyanines*, *19*(01–03), 45–64. https://doi.org/10.1142/S1088424615300013

McKeown, N. B. (1998). *Phthalocyanine Materials: Synthesis, Structure and Function*. Cambridge University Press.

Meng, X., Eluagwule, B., Wang, M., Wang, L., & Zhang, J. (2020). 9—Solar photocatalysis for environmental remediation. In C. Mustansar Hussain & A. K. Mishra (Eds.), *Handbook of Smart Photocatalytic Materials* (pp. 183–195). Elsevier. https://doi.org/10.1016/B978-0-12-819049-4.00013-1

Menne, M. J., Williams, C. N., Gleason, B. E., Rennie, J. J., & Lawrimore, J. H. (2018). The Global Historical Climatology Network Monthly Temperature Dataset, Version 4. *Journal of Climate*, *31*(24), 9835–9854. https://doi.org/10.1175/JCLI-D-18-0094.1

Plint, T., Lessard, B. H., & Bender, T. P. (2016). Assessing the potential of group 13 and 14 metal/metalloid phthalocyanines as hole transport layers in organic light emitting diodes. *Journal of Applied Physics*, *119*(14), 145502. https://doi.org/10.1063/1.4945377

Portmann, R. W., Daniel, J. S., & Ravishankara, A. R. (2012). Stratospheric ozone depletion due to nitrous oxide: Influences of other gases. *Philosophical Transactions of the Royal Society B: Biological Sciences*, *367*(1593), 1256–1264. https://doi.org/10.1098/rstb.2011.0377

Qin, D., Zhou, Y., Wang, W., Zhang, C., Zeng, G., Huang, D., Wang, L., Wang, H., Yang, Y., Lei, L., Chen, S., & He, D. (2020). Recent advances in two-dimensional nanomaterials for photocatalytic reduction of CO2: Insights into performance, theories and perspective. *Journal of Materials Chemistry A*, *8*(37), 19156–19195. https://doi.org/10.1039/D0TA07460H

Rao, C. N. R., & Lingampalli, S. R. (2016). Generation of Hydrogen by Visible Light-Induced Water Splitting with the Use of Semiconductors and Dyes. *Small*, *12*(1), 16–23. https://doi.org/10.1002/smll.201500420

Rosa, E. V., Campos, A. F. C., Rodrigues, M. O., Henini, M., & Sousa, M. H. (2023). 4—Nano-engineered composites based on carbon nitride as potential agents for the remediation of water with micropollutants. In M. Henini & M. O. Rodrigues (Eds.), *Quantum Materials, Devices, and Applications* (pp. 87–115). Elsevier. https://doi.org/10.1016/B978-0-12-820566-2.00006-5

Roy, S., Miller, M., Warnan, J., Leung, J. J., Sahm, C. D., & Reisner, E. (2021). Electrocatalytic and Solar-Driven Reduction of Aqueous CO$_2$ with Molecular Cobalt Phthalocyanine–Metal Oxide Hybrid Materials. *ACS Catalysis*, *11*(3), 1868–1876. https://doi.org/10.1021/acscatal.0c04744

Roy, S., & Reisner, E. (2019). Visible-Light-Driven CO2 Reduction by Mesoporous Carbon Nitride Modified with Polymeric Cobalt Phthalocyanine. *Angewandte Chemie International Edition*, *58*(35), 12180–12184. https://doi.org/10.1002/anie.201907082

Sakamoto, K., & Ohno-Okumura, E. (2009). Syntheses and Functional Properties of Phthalocyanines. *Materials*, *2*(3), 1127–1179. https://doi.org/10.3390/ma2031127

Santhanaraghavan, P., & Ramasamy, P. (2001). ADP- and KTP-type Crystals: Growth, Characterization, and Applications. In K. H. J. Buschow, R. W. Cahn, M. C. Flemings, B. Ilschner, E. J. Kramer, S. Mahajan, & P. Veyssière (Eds.), *Encyclopedia of Materials: Science and Technology* (pp. 53–59). Elsevier. https://doi.org/10.1016/B0-08-043152-6/00010-3

Shang, B., Zhao, F., Choi, C., Jia, X., Pauly, M., Wu, Y., Tao, Z., Zhong, Y., Harmon, N., Maggard, P. A., Lian, T., Hazari, N., & Wang, H. (2022). Monolayer Molecular Functionalization Enabled by Acid–Base Interaction for High-Performance Photochemical CO2 Reduction. *ACS Energy Letters*, *7*(7), 2265–2272. https://doi.org/10.1021/acsenergylett.2c01147

Shi, H., Chen, G., Zhang, C., & Zou, Z. (2014). Polymeric g-C3N4 Coupled with NaNbO3 Nanowires toward Enhanced Photocatalytic Reduction of CO2 into Renewable Fuel. *ACS Catalysis*, *4*(10), 3637–3643. https://doi.org/10.1021/cs500848f

Tariq, W., Nasir, A., Arslan, C., Rashid, H., Sarmad, M., & Gillani, S. H. (2023). Chapter 16—Photocatalytic reduction of highly toxic lead and cadmium from aqueous solution. In A. Ahmad, R. Kumar, & M. Jawaid (Eds.), *Emerging Techniques for Treatment of Toxic Metals from Wastewater* (pp. 399–427). Elsevier. https://doi.org/10.1016/B978-0-12-822880-7.00019-4

Thomas, A. L. (1990). *Phthalocyanine Research and Applications*. CRC Press.

Tian, J., Liu, Q., Asiri, A. M., Sun, X., & He, Y. (2015). Ultrathin graphitic C3N4 nanofibers: Hydrolysis-driven top-down rapid synthesis and application as a novel fluorosensor for rapid, sensitive, and selective detection of Fe3+. *Sensors and Actuators B: Chemical*, *216*, 453–460. https://doi.org/10.1016/j.snb.2015.04.075

Tkáčová, K., Heegn, H., & Števulová, N. (1993). Energy transfer and conversion during comminution and mechanical activation. *International Journal of Mineral Processing*, *40*(1), 17–31. https://doi.org/10.1016/0301-7516(93)90037-B

Tsuzuki, T. (2021). Mechanochemical synthesis of metal oxide nanoparticles. *Communications Chemistry*, *4*(1), Article 1. https://doi.org/10.1038/s42004-021-00582-3

Undavalli, V. K., Ling, C., & Khandelwal, B. (2021). Chapter 6—Impact of alternative fuels and properties on elastomer compatibility. In B. Khandelwal (Ed.), *Aviation Fuels* (pp. 113–132). Academic Press. https://doi.org/10.1016/B978-0-12-818314-4.00001-7

Wang, H., Bian, Y., Hu, J., & Dai, L. (2018). Highly crystalline sulfur-doped carbon nitride as photocatalyst for efficient visible-light hydrogen generation. *Applied Catalysis B: Environmental*, *238*, 592–598. https://doi.org/10.1016/j.apcatb.2018.07.023

Wang, Y., Wang, Y., Chen, Y., Yin, C., Zuo, Y., & Cui, L.-F. (2015). Synthesis of Ti-doped graphitic carbon nitride with improved photocatalytic activity under visible light. *Materials Letters*, *139*, 70–72. https://doi.org/10.1016/j.matlet.2014.10.008

Xiao, Y., Zhang, L., Peng, F., & Pan, G.-B. (2018). Fabrication of a cobalt phthalocyanine free-standing film on an ionic liquid surface for memory device applications. *RSC Advances*, *8*(10), 5344–5349. https://doi.org/10.1039/C7RA12953J

Yan, S. C., Li, Z. S., & Zou, Z. G. (2009). Photodegradation performance of g-C3N4 fabricated by directly heating melamine. *Langmuir: The ACS Journal of Surfaces and Colloids*, *25*(17), 10397–10401. https://doi.org/10.1021/la900923z

Yuen, A. P., Jovanovic, S. M., Hor, A.-M., Klenkler, R. A., Devenyi, G. A., Loutfy, R. O., & Preston, J. S. (2012). Photovoltaic properties of M-phthalocyanine/fullerene organic solar cells. *Solar Energy*, *86*(6), 1683–1688. https://doi.org/10.1016/j.solener.2012.03.019

Zhou, Y., Zhang, L., Huang, W., Kong, Q., Fan, X., Wang, M., & Shi, J. (2016). N-doped graphitic carbon-incorporated g-C3N4 for remarkably enhanced photocatalytic H2 evolution under visible light. *Carbon*, *99*, 111–117. https://doi.org/10.1016/j.carbon.2015.12.008